Journal of Pharmacological Sciences 128 (2015) 1–7

HOSTED BY

ELSEVIER

Contents lists available at ScienceDirect

Journal of Pharmacological Sciences

journal homepage: www.elsevier.com/locate/jphs

Current perspective

New light on ion channel imaging by total internal reflection fluorescence (TIRF) microscopy

Hisao Yamamura*, Yoshiaki Suzuki, Yuji Imaizumi

Department of Molecular & Cellular Pharmacology, Graduate School of Pharmaceutical Sciences, Nagoya City University, Nagoya 467-8603, Japan

ARTICLE INFO

Article history:
Received 14 February 2015
Received in revised form
30 March 2015
Accepted 6 April 2015
Available online 15 April 2015

Keywords:
TIRF imaging
Single-molecule imaging
Ion channel
FRET
Subunit stoichiometry

ABSTRACT

Ion channels play pivotal roles in a wide variety of cellular functions; therefore, their physiological characteristics, pharmacological responses, and molecular structures have been extensively investigated. However, the mobility of an ion channel itself in the cell membrane has not been examined in as much detail. A total internal reflection fluorescence (TIRF) microscope allows fluorophores to be imaged in a restricted region within an evanescent field of less than 200 nm from the interface of the coverslip and plasma membrane in living cells. Thus the TIRF microscope is useful for selectively visualizing the plasmalemmal surface and subplasmalemmal zone. In this review, we focused on a single-molecule analysis of the dynamic movement of ion channels in the plasma membrane using TIRF microscopy. We also described two single-molecule imaging techniques under TIRF microscopy: fluorescence resonance energy transfer (FRET) for the identification of molecules that interact with ion channels, and subunit counting for the determination of subunit stoichiometry in a functional channel. TIRF imaging can also be used to analyze spatiotemporal Ca^{2+} events in the subplasmalemma. Single-molecule analyses of ion channels and localized Ca^{2+} signals based on TIRF imaging provide beneficial pharmacological and physiological information concerning the functions of ion channels.

1. Introduction

The activity of ion channels is critical for determining diverse biogenic functions in various types of cells. The molecular structures, pharmacological characteristics, and physiological/pathological significance of ion channels have been extensively studied for many decades. Although many types of ion channels are present in the cell membrane and mediate a large number of cellular processes, their dynamics and organization in the plasma membrane have not yet been elucidated in detail. Difficulties have been associated with imaging molecular mobility using traditional epifluorescence or confocal microscopy, because specific fluorescent signals on the surface of the plasma membrane are easily obscured by fluorescence originating from the bulk of the cell. Recent advances in fluorescence microscopy have enabled imaging at the single-molecule level in living cells. A total internal reflection fluorescence (TIRF) microscope with high spatial resolution and fast scanning is now used to investigate the localization and dynamics of ion channels in the plasma membrane in living cells.

In this review, we focused on the molecular dynamics of single ion channels in the membrane surface of cells using TIRF microscopy with fluorescent probes and fluorescent-tagged proteins. We also described how to identify molecules interacting with ion channels by fluorescence resonance energy transfer (FRET) analysis at the single-molecule level under TIRF microscopy. Furthermore, we summarize the subunit counting method based on single-molecule photobleaching under TIRF microscopy that is used to determine subunit stoichiometry in a functional channel. TIRF imaging for spatiotemporal Ca^{2+} events such as Ca^{2+} sparklets, Ca^{2+} hotspots, and Ca^{2+} sparks has also been reviewed.

2. TIRF microscopy

A TIRF microscope (also known as an evanescent field microscope) uses an evanescent field to selectively illuminate and excite fluorophores in a restricted region immediately adjacent to the

* Corresponding author. Department of Molecular & Cellular Pharmacology, Graduate School of Pharmaceutical Sciences, Nagoya City University, 3-1 Tanabedori Mizuhoku, Nagoya 467-8603, Japan. Tel.: +81 52 836 3433; fax: +81 52 836 3432.
E-mail address: yamamura@phar.nagoya-cu.ac.jp (H. Yamamura).

Peer review under responsibility of Japanese Pharmacological Society.

http://dx.doi.org/10.1016/j.jphs.2015.04.004

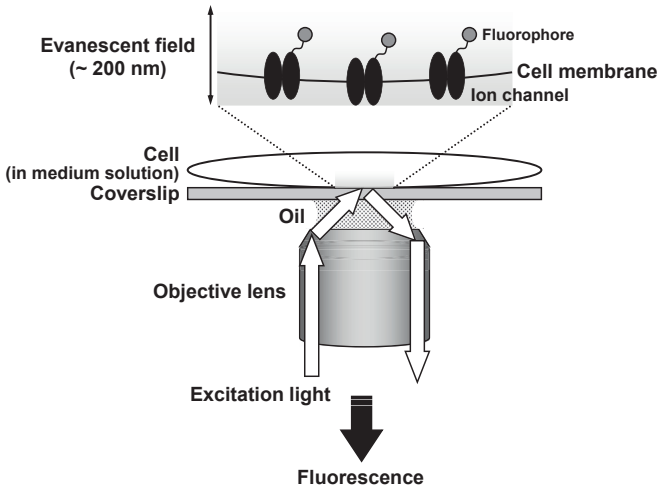

Fig. 1. Diagram of single-molecule imaging using a TIRF microscope. A TIRF microscope uses an evanescent field that is generated when excitation light is totally internally reflected at the interface between glass (coverslip on which cells are grown) and water (medium solution immersing the cell membrane and subplasmalemmal region). Thus, a TIRF microscope enables the distribution and movement of functional membrane proteins, including ion channels labeled with fluorophores, to be detected at the single-molecule level in a restricted region within less than 200 nm from the interface in living cells. Spatiotemporal Ca^{2+} signals can also be imaged with fluorescent Ca^{2+} indicators using a TIRF microscope.

interface between glass (coverslip on which cells are grown) and water (medium solution immersing the cell) (Fig. 1) (1). The evanescent field is only generated when the incident light is totally internally reflected at the glass–water interface. According to the laws of optics, when an angle is larger than the critical angle determined by the ratio of the two refractive indices (glass and water), the incident light is not primarily transmitted to the second medium. The incident light is instead reflected, whereas all the light energy is not. The component penetrating into the second medium is referred to as an evanescent field. The fluorescent probes and fluorescent-tagged proteins are excited by an evanescent light in close proximity to the coverslip. The evanescent light decays exponentially with increase in the distance from the interface between the coverslip and medium, and thus, selectively illuminates only the thin section (less than 200 nm) of the cell in contact with the coverslip, including the plasma membrane (which are approximately 7~10 nm in thickness) and cytoplasmic region immediately beneath the plasma membrane. In addition, background fluorescence is minimized because fluorophores located further away from the coverslip are rarely excited. Therefore, TIRF microscopy allows single fluorescent-labeled molecules at the level of the plasmalemma and subplasmalemma in living cells to be visualized in a limited TIRF zone less than 200 nm from the chamber bottom.

The dynamical processes of receptors and signal transduction molecules have been observed at the level of a single-molecule in living cells using TIRF microscopy. Molecules of interest are labeled with small organic dyes (Cy5, FITC, Alexa) and quantum dots as well as fluorescence proteins (CFP, GFP, YFP) (2). The movement of a motor protein, DNA transcription, receptor signaling, membrane architecture, and insulin exocytosis have so far been imaged at the level of single molecules using TIRF microscopy (3–5). TIRF microscopy can be used in a wide range of cell physiological applications, and is particularly suited for the analysis of the localization and dynamics of molecules in the plasma membrane. In living cells, the ability to selectively detect a single molecule or clusters (or a small number of molecules) is a powerful method that allows for a deeper understanding of the dynamics involved in cellular organization.

3. Single-molecule imaging using TIRF microscopy

In contrast to single-molecule analysis for receptors and signal transductions, the dynamic behaviors of ion channels have not yet been investigated extensively. The distribution and molecular behavior of single ion channels in the membrane surface of living cells were visualized by TIRF imaging (Fig. 2). The diffusion coefficients of several types of ion channels, obtained from TIRF imaging, are summarized in Table 1: Na^+ channels (6), transient receptor potential (TRP) channels (7–9), Cl^- channels (10–12), and aquaporin water channels (13, 14) in addition to K^+ channels (15, 16). Although it is difficult to compare these diffusion coefficients under different experimental conditions, the mobility of fluorescent-labeled ion channels in reconstituted cells only represents one-thousandth the value of that in a lipid bilayer environment (17). Similar analyses for ion channels have been performed using other microscopic techniques with the same precision, including the fluorescence recovery after photobleaching (FRAP) method (2, 18) under confocal microscopy for K^+ channels (19), Ca^{2+} channels (20), and Cl^- channels (21, 22).

Several studies reported that the molecular behavior of ion channels was more restricted by auxiliary subunits (16, 23), cytoskeleton and scaffold proteins (6, 11, 16, 24), and region of the cell (20, 25) than expected from the molecular size of the ion channels. Moreover, the behavior of ion channels in intact cells is known to be more complex than that in cell lines. Our previous findings showed that the molecular movement of single ion channels in vascular smooth muscle cells was markedly slower than that in HEK293 cells (16). On the other hand, previous studies found no significant

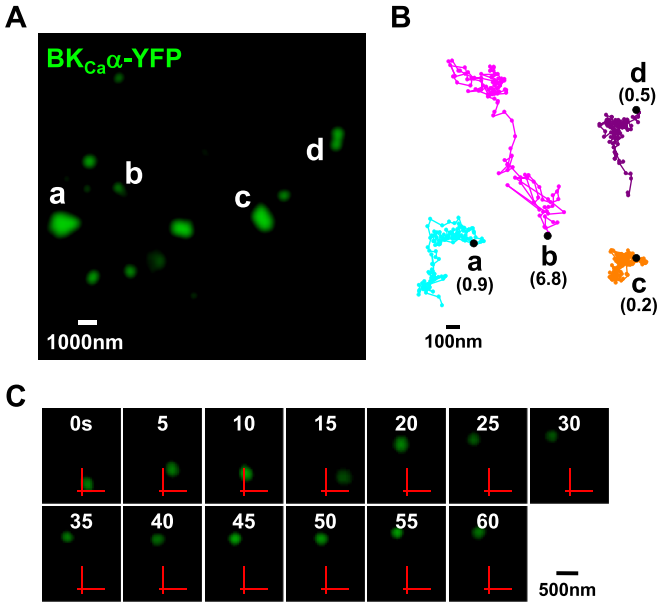

Fig. 2. Single-molecule imaging of BK_{Ca} channels using TIRF microscopy. The localization and behavior of single $BK_{Ca}\alpha$ ($K_{Ca}1.1$) subunit molecules in the plasma membrane were imaged using TIRF microscopy. $BK_{Ca}\alpha$-YFP was transiently expressed in HEK293 cells. (A) Representative TIRF image of a HEK293 cell expressing $BK_{Ca}\alpha$-YFP. Single channels or clusters of $BK_{Ca}\alpha$-YFP were observed in the TIRF region. (B) Single $BK_{Ca}\alpha$-YFP molecules on the membrane surface, indicated by the image in A (particles a–d), were tracked for 60 s. Values for the diffusion coefficient of fluorescent particles for 10 s are given in parentheses ($\times 10^3$ nm^2/s). Black dots indicate the starting points of tracking. (C) The dynamic mobility of a $BK_{Ca}\alpha$-YFP molecule (particle b in A and B) was imaged every 5 s. [Modified from (16)].

Table 1
Diffusion coefficients of several types of ion channels.

Ion channel	Size (KDa)	Diffusion coefficient ($\times 10^3$ nm^2/s)	Probe	Cell type	Reference
$K_{Ca}1.1/BK_{Ca}\alpha$	138	3000	Cy5	Lipid bilayer	(17)
$K_{Ca}1.1/BK_{Ca}\alpha$	138	6.7	YFP	HEK293	(16)
$K_{Ca}1.1/BK_{Ca}\alpha$	138	0.29	YFP	Vascular SMC	(16)
$BK_{Ca}\beta1$	22	3.9	CFP	HEK293	(16)
$BK_{Ca}\alpha\beta1$	138, 22	2.5	YFP/CFP	HEK293	(16)
$K_{Ca}3.1/IK_{Ca}$	48	67.3	Qdot 655	MDCK-F	(15)
$K_{Ca}3.1/IK_{Ca}$	48	139	Alexa 488	MDCK-F	(15)
ENaC$\alpha\beta\gamma$	76, 73, 74	0.078	eYFP	COS-7	(6)
TRPC5	111	0.019	eGFP	HEK293	(7)
TRPV5	83	0.2~1	eGFP	MDCK	(8)
TRPM8	128	1.68~10.7	eGFP	HEK293T, F11	(9)
CFTR	168	5	Qdot 655	COS-7	(10)
CFTR	168	4	Qdot 655	COS-7, MDCK II	(11)
GlyRα3	54	130	Alexa 647	HEK293	(12)
AQP1	29	25~84	Qdot 655	COS-7, MDCK	(14)
AQP1	29	30~81	Qdot 655	COS-7, MDCK	(13)
AQP4	35	60	Qdot 655	COS-7, MDCK	(13)
AQP4	35	6~50	Qdot 655	Astrocyte	(13)

$K_{Ca}1.1/BK_{Ca}$, large-conductance Ca^{2+}-activated K^+ channel.
$K_{Ca}3.1/IK_{Ca}$, intermediate-conductance Ca^{2+}-activated K^+ channel.
ENaC, epithelial Na^+ channel.
TRPC5, transient receptor potential channel canonical subfamily 5.
TRPV5, transient receptor potential channel vanilloid subfamily 5.
TRPM8, transient receptor potential channel melastatin subfamily 8.
CFTR, cystic fibrosis transmembrane conductance regulator (Cl^- channel).
GlyR, glycine receptor (Cl^- channel).
AQP, aquaporin (water channel).
SMC, smooth muscle cell.
CFP/GFP/YFP = 27 KDa.

difference in molecular behaviors between cell lines and intact cells (13, 19, 21, 26). The reason for this discrepancy currently remains unknown, but may be attributed to differences in types of cells.

The large-conductance Ca^{2+}-activated K^+ (BK_{Ca}, also known as $K_{Ca}1.1$) channel is a tetrameric assembly of pore-forming α-subunits with four auxiliary β-subunits. The $BK_{Ca}\beta$ subunit binds with the $BK_{Ca}\alpha$ subunit in a one-to-one manner, and modulates Ca^{2+} sensitivity, voltage dependence, and pharmacological responses. The $BK_{Ca}\beta$ subunit has a tissue-specific distribution and is responsible for tissue-specific variations in the characteristics of the BK_{Ca} channel (27, 28). A cotransfection experiment with $BK_{Ca}\alpha$-YFP and $BK_{Ca}\beta1$-CFP cDNAs at a ratio of 1:1 into HEK293 cells did not lead to all $BK_{Ca}\alpha$-YFP being colocalized with $BK_{Ca}\beta1$-CFP (64% of particles). It is noteworthy that $BK_{Ca}\alpha$ alone (30%) and $BK_{Ca}\beta1$ (6%) were distributed independently of each other on the plasma membrane in HEK293 cells (16). Functional $BK_{Ca}\alpha\beta2$ currents under whole cell or single-channel configurations in *Xenopus* oocytes were previously shown to be formed with less than four $BK_{Ca}\beta2$ subunits per tetrameric $BK_{Ca}\alpha$ channel (29). Furthermore, 17β-estradiol, a selective opener for the $BK_{Ca}\beta1$ subunit, did not always produce the expected responses in HEK293F cells (30). These contradictory findings may be attributed to, at least in a heterologous expression system, a small number of BK_{Ca} channels consisting of $BK_{Ca}\alpha$ subunits without coupling to $BK_{Ca}\beta$ subunits, even if equally cotransfected. Therefore, we require careful attention when performing cotransfection experiments in reconstituted expression systems.

4. FRET analysis under TIRF microscopy

FRET is an optical phenomenon of energy transfer from an excited fluorophore (donor) to another fluorophore (acceptor) when the acceptor is close to the donor (1~10 nm) (18, 31). The efficiency of FRET is inversely proportional to the sixth power of the distance between the donor and acceptor based on the Förster equation. Numerous methods have been used to measure FRET. The most direct method for measuring the efficiency of FRET is to monitor changes in donor fluorescence before and after photobleaching of the acceptor. FRET efficiency is calculated as a percentage increase in the emission of the donor fluorophore (CFP)

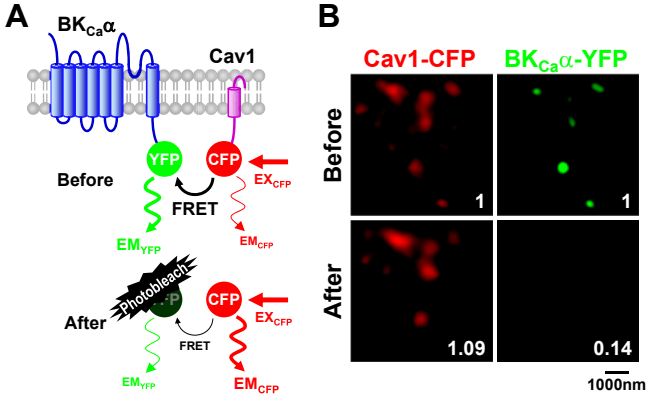

Fig. 3. TIRF/FRET analysis based on the acceptor bleaching method. The molecular interaction between BK_{Ca} channels and caveolin 1 (Cav1) molecules was examined using FRET analysis under a TIRF microscope. (A) Diagram of the concept of FRET analysis based on the acceptor bleaching method. $BK_{Ca}\alpha$-YFP and Cav1-CFP were transiently coexpressed in HEK293 cells. When $BK_{Ca}\alpha$-YFP and Cav1-CFP were located closely to each other within ~10 nm, YFP emission (EM_{YFP}, 527 nm) was detected by CFP excitation (EX_{CFP}, 405 nm) via FRET. After FRET disruption by YFP photobleaching, the same CFP excitation caused the stronger emission of CFP (EM_{CFP}, 475 nm) than that before YFP photobleaching. (B) Representative TIRF images of a vascular smooth muscle cell expressing $BK_{Ca}\alpha$-YFP and Cav1-CFP are shown. Images were obtained before and after YFP photobleaching. The values in each image indicate fluorescence intensity relative to that before photobleaching. FRET efficiency was calculated as a percentage increase in CFP emission after YFP photobleaching using the following equation: FRET (%) = $[(CFP_{after}-CFP_{before})/CFP_{after}] \times 100$, where CFP_{after} and CFP_{before} are CFP emissions after and before YFP photobleaching, respectively. FRET efficiency between $BK_{Ca}\alpha$-YFP and Cav1-CFP in this myocyte was 8.2%. [Modified from (16)].

after photobleaching of the acceptor (YFP) according to the following equation: FRET (%) = [(CFP_{after}−CFP_{before})/CFP_{after}] × 100, where CFP_{after} and CFP_{before} are CFP emissions after and before YFP photobleaching, respectively. To obtain accurate FRET measurements, this technique requires complete bleaching of the acceptor (which can take several minutes) without bleaching the donor. An advantage of acceptor bleaching analysis is that only a change in donor fluorescence is used to calculate the efficiency of FRET, making it possible to compare FRET efficiencies among different studies. One potential disadvantage of acceptor bleaching analysis is the movement of fluorophores during the bleaching period. This is a matter of concern with TIRF microscopy, in which fluorophores located in the cytoplasmic region (not excited) can move to the plasma membrane during the bleaching time (subsequently becoming excited). To avoid this, cells are typically fixed with paraformaldehyde before acceptor bleaching experiments. Separating from several biochemical approaches, the acceptor photobleaching method is widely used to detect protein–protein interactions.

Functional interactions and assemblies have been identified between ion channels using a combination of FRET and TIRF microscopy: ATP-gated $P2X_2$ and α4β2 nicotinic channels (32); homo/heteromeric voltage-dependent K^+ (KCNQ/K_V7) channels (33); homo/heteromeric transient receptor potential canonical channels (TRPC4 and TRPC5) (34); transient receptor potential vanilloid (TRPV) 1 and transient receptor potential ankyrin (TRPA) 1 channels (35); the BK_{Ca} channel and voltage-dependent Ca^{2+} channel (VDCC) α1C subunit (also known as Ca_V1.2) (36) in the plasma membrane. TIRF/FRET analysis can also detect molecular assemblies and signal complexes including ion channels: G protein-coupled K^+ channels (GIRK/K_{ir}3) during Gβγ subunit activation (37, 38); the GIRK/K_{ir}3 channel and $GABA_B$ receptor (39); the KCNQ/K_V7 channel, calmodulin, and A-kinase anchoring protein (AKAP79/150) (40, 41); VDCCα1C and Ca_Vβ (42); the BK_{Ca} channel and caveolin 1 (Fig. 3) (16); the BK_{Ca} channel and caveolin 3 (43); VDCC (Ca_V1.2, Ca_V1.3, Ca_V2.3) and RalA GTPase (44); and VDCCα1C and caveolin 1 (36). The acceptor photobleaching method is widely used to visualize and quantify protein–protein interactions in real-time with subcellular resolution.

5. Subunit stoichiometry of ion channels using single-molecule photobleaching

The subunit number and stoichiometry of functional membrane proteins are difficult to determine without disrupting the membrane environment. We herein described single-molecule imaging to count the subunits of proteins in living cell membranes by observing the bleaching steps of GFP fused to the proteins of interest. The photobleaching of GFP fluorescence in a whole cell gradually occurs with time, whereas the photobleaching of a single GFP involves a discrete process in an all-or-none manner. Therefore, the fluorescence intensity of a protein complex with one or several

Table 2
Subunit stoichiometry of ion channels in a channel complex.

Ion channel	Stoichiometry	Tag	Cell type	Reference
Ca_V2.3/VDCCα1E	1	eGFP	*Xenopus* oocyte	(45)
Ca_V1.2/VDCCα1C	1	eGFP	*Xenopus* oocyte	(46)
Ca_V1.2/VDCCα1C	1	GFP	HEK293	(36)
KCNQ1/K_V7.1	4	eGFP	*Xenopus* oocyte	(47)
KCNQ1 + KCNE1	4:1~4:4	eGFP, mCherry	*Xenopus* oocyte	(47)
K_{Ca}1.1/BK_{Ca}α	4	GFP	HEK293	(16)
TRPM8	4	eGFP	HEK293T, F11	(9)
Orai1	4 (activated)	eGFP	HEK293	(55)
Orai1	2 (resting), 4 (activated)	eGFP	*Xenopus* oocyte	(48)
Orai1, 3	2 (resting), 4 (activated)	eGFP	HEK293	(54)
X-fA4 (CNG)	4	eGFP	*Xenopus* oocyte	(45)
HCN2 + TRIP8b	4:4	eGFP	*Xenopus* oocyte	(57)
ASIC1a, 2a	3	eGFP	*Xenopus* oocyte	(49)
ASIC1a + ASIC2a	2:1 or 1:2	eGFP	*Xenopus* oocyte	(49)
NMDA (NR1 + NR2B)	2:2	eGFP	*Xenopus* oocyte	(45)
NMDA (NR1 + NR3B)	2:2	eGFP	*Xenopus* oocyte	(45)
TRPP2 + PKD1	3:1	eGFP, mCherry	*Xenopus* oocyte	(58)
TRPP3	3	eGFP	*Xenopus* oocyte	(50)
TRPP3 + PKD1L3	3:1	eGFP, mCherry	*Xenopus* oocyte	(50)
CFTR	1	GFP	CHO–K1, COS-7	(56)
Best1, 2, 3, 4	4	eGFP	*Xenopus* oocyte	(51)
TMEM16A	2	GFP	HEK293	(61)
GlyR (GlyRα)	5	eGFP	*Xenopus* oocyte	(52)
GlyR (GlyRα + GlyRβ)	3:2	Venus	*Xenopus* oocyte	(52)
H_V1	2	eGFP	*Xenopus* oocyte	(53)

Ca_V/VDCC voltage-dependent Ca^{2+} channel.
KCNQ and KCNE, voltage-dependent K^+ channel (K_V7) and its auxiliary subunit, respectively.
K_{Ca}1.1/BK_{Ca}, large-conductance Ca^{2+}-activated K^+ channel.
TRPM8, transient receptor potential channel melastatin subfamily 8.
CNG, cyclic nucleotide-gated channel.
HCN, hyperpolarization-activated cyclic nucleotide-gated channel.
TRIP8b, tetratricopeptide repeat-counting Rab8b-interating protein.
ASIC, acid-sensing ion channel.
NMDA, N-methyl-D-aspartate receptor (glutamate receptor, non-selective cation channel).
PKD, polycystic kidney disease.
TRPP, transient receptor potential polycystic subfamily.
CFTR, cystic fibrosis transmembrane conductance regulator (Cl^- channel).
Best, bestrophin (Cl^- channel).
GlyR, glycine receptor (Cl^- channel).
H_V1, voltage-gated H^+ channel.

GFP molecules decreases in a stepwise fashion. The number of steps indicates the number of GFP-tagged subunits in the complex. Based on this principle, the number of subunits in an ion channel component and its complex can be directly determined by counting the number of discrete steps involved in photobleaching single fluorescent molecules using TIRF microscopy (45).

The subunit stoichiometry of ion channels obtained by GFP photobleaching analysis under TIRF microscopy in *Xenopus* oocytes are summarized in Table 2: VDCCs (45, 46), K^+ channels (47), store-operated Ca^{2+} (SOC) channels (48), cyclic nucleotide-gated channels, non-selective cation channels (45), acid-sensing ion channels (49), TRP channels (50), Cl^- channels (51, 52), and H^+ channels (53). Several groups applied this elegant technique to ion channels in mammalian cell lines, including TRP channels (9), SOC channels (54, 55), and Cl^- channels (56). Furthermore this analysis has revealed the assembly and stoichiometry of the pore-forming subunit and its auxiliary subunit (47, 57) as well as its heteromeric component (45, 49, 50, 52, 58).

We also performed subunit counting experiments on the BK_{Ca} channel and VDCC in the plasma membrane of HEK293 cells. Single-molecule photobleaching analysis revealed that $BK_{Ca}\alpha$ subunits were composed of a tetramer in a single BK_{Ca} channel (Fig. 4A) (16) while VDCCα1C subunits were composed of a monomer in a single channel (Fig. 4B) (36). After testing this method with these proteins of known stoichiometry, we elucidated the subunit composition of the novel Ca^{2+}-activated Cl^- (Cl_{Ca}) channel, TMEM16A. TMEM16A is expressed as a Cl_{Ca} channel in various tissues and is expected to regulate their functions (59, 60). Its subunit stoichiometry had yet to be clarified: how many subunits form a functional Cl_{Ca} channel had yet to be determined. Our single-molecule photobleaching analysis revealed that the homodimers of TMEM16A may determine the features of Cl_{Ca} activity (Fig. 4C). To the best of our knowledge, this finding demonstrated for the first time in a living cell that TMEM16A molecules preferentially formed dimers in a functional channel (61). The single-molecule photobleaching method under TIRF microscopy provides a tool for quickly determining the subunit stoichiometry of membrane proteins in living cells by counting the bleaching steps of GFP tags.

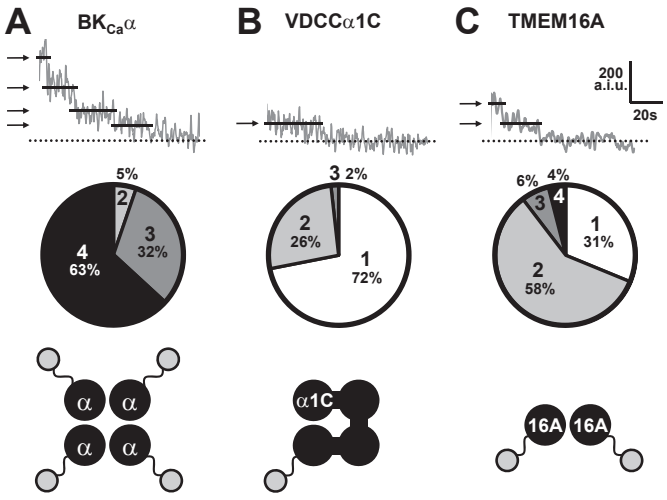

Fig. 4. Subunit stoichiometry of ion channels using the GFP photobleaching technique under TIRF microscopy. The $BK_{Ca}\alpha$-GFP, VDCCα1C-GFP, or TMEM16A-GFP subunit was transiently expressed in HEK293 cells. Based on the single-molecule photobleaching method, the bleaching steps of GFP signals in a TIRF region were counted in order to determine the number of these subunits within a single fluorescent particle. Representative traces in the fluorescent intensity of the $BK_{Ca}\alpha$ (A), VDCCα1C (B), or TMEM16A (C) channel after the photobleaching stimulation were plotted (*upper*). Arrows and solid lines indicate bleaching step(s). The dotted line indicates the complete bleaching (basal) level. The number of bleaching steps and proportion (%) in HEK293 cells expressing these subunits was summarized (*middle*). The subunit stoichiometry estimated by these results was shown (*bottom*). $BK_{Ca}\alpha$ and VDCCα1C subunits were expressed as a tetramer and monomer, respectively, in the plasma membrane. Moreover, this analysis revealed that the novel Cl_{Ca} channel component, TMEM16A, potentially formed a dimer. [Modified from (16, 36, 61)].

6. Spatiotemporal Ca^{2+} imaging using TIRF microscopy

The cytosolic Ca^{2+} concentration ($[Ca^{2+}]_{cyt}$) is an important factor that regulates a wide range of physiological functions including gene expression, cell proliferation, neurotransmitter release, hormone secretion, and muscle contraction. Changes in cytosolic Ca^{2+} signaling were shown to be reorganized in order to vary both spatially and temporally in various types of cells (Fig. 5) (62). For example, Ca^{2+} influx through nicotinic channels in *Xenopus* oocytes was imaged with a Ca^{2+} indicator using a TIRF microscope (63). A Ca^{2+} sparklet, a fluorescent image of the influx of Ca^{2+} through Ca^{2+}-permeable channels including VDCCs, was imaged with Fluo-5F in vascular smooth muscle cells using a TIRF microscope (64). In addition, the elementary unit of SOC entry mediated by a direct interaction between STIM1 molecules in the endoplasmic reticulum (ER) and Orai1 channels in the plasma membrane was clearly shown in Jurkat cells using TIRF microscopy (65).

In smooth muscle cells, we successfully imaged depolarization-evoked local Ca^{2+} transients through ryanodine receptors (RyRs) in the subplasmalemmal sarcoplasmic reticulum (SR), termed as Ca^{2+} hotspots, using fast-scanning confocal fluorescent microscopy (66–69). Ca^{2+} hotspots activated the BK_{Ca} channels in the plasma membrane, thereby contributing to the repolarization phase of an action potential in smooth muscle cells. However, it was difficult to separate the component of Ca^{2+} influx through VDCCs from local Ca^{2+} transients evoked by depolarization at a lower spatial resolution of confocal imaging (0.33 × 0.27 μm per pixel and 1.2~1.5 μm to Z-axis direction). On the other hand, TIRF imaging with higher spatial resolution (178 × 178 nm per pixel and less than 200 nm to

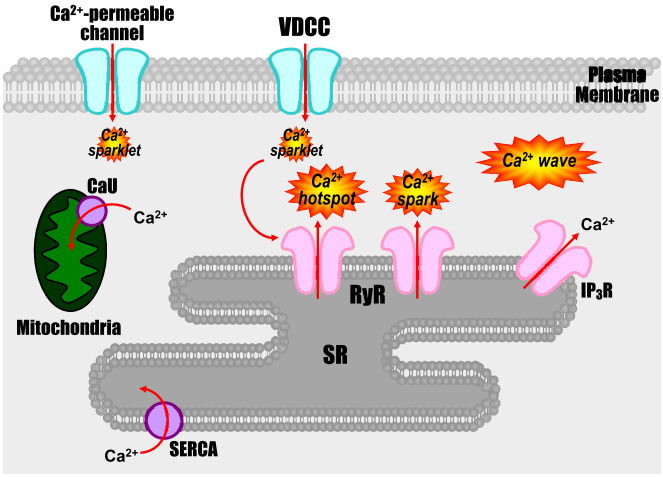

Fig. 5. Spatiotemporal Ca^{2+} signaling. Changes in $[Ca^{2+}]_{cyt}$ vary spatially and temporally in various types of cells. A Ca^{2+} sparklet is a fluorescent image of the influx of Ca^{2+} through the Ca^{2+}-permeable channels and VDCCs. A Ca^{2+} hotspot is a fluorescent image of ClCR from RyR on the SR. A Ca^{2+} sparklet may represent a trigger while a Ca^{2+} hotspot is an amplification mechanism underlying smooth muscle contraction. A Ca^{2+} spark is a fluorescent image of spontaneous Ca^{2+} release from RyR on the SR. A Ca^{2+} spark contributes to the regulation of smooth muscle tone. Abbreviations: CaU, Ca^{2+} uniporter; IP_3R, IP_3 receptor; RyR, ryanodine receptor; SERCA, SR/ER Ca^{2+} ATPase; SR, sarcoplasmic reticulum; VDCC, voltage-dependent Ca^{2+} channel.

Z-axis direction) clearly visualized the depolarization-evoked influx of Ca^{2+} through VDCCs (Ca^{2+} sparklets through single or clustered L-type VDCCs) prior to Ca^{2+}-induced Ca^{2+} release (CICR, Ca^{2+} hotspots) in smooth muscle cells (70). Alternatively, a typical example of a spatiotemporal Ca^{2+} event is likely to be Ca^{2+} sparks. A Ca^{2+} spark is due to a spontaneous Ca^{2+} release from a single Ca^{2+} release unit, or RyR on the SR. In smooth muscle cells, Ca^{2+} sparks play crucial roles in the regulation of smooth muscle tone (62,71–73). We also imaged Ca^{2+} sparks using TIRF microscopy (74, 75). The physiological and pathological significance of spatiotemporal Ca^{2+} events in various tissues have yet to be clarified.

7. Conclusions

TIRF microscopy is now widely used to observe the fluorescence of a single molecule and localized Ca^{2+} signaling, making it a valuable tool in the fields of biophysics and cell biology. According to the PubMed database, over 1500 publications on 'total internal reflection fluorescence' have been published since the development of the TIRF microscope in the 1980s, and approximately 200 studies are added to the database every year. The single-molecule analysis of ion channels by means of TIRF imaging, FRET analysis, and subunit counting after photobleaching in living cells has provided useful physiological and pathological information on ion channel functions and a functionally-coupled molecular complex in the cell membrane. In addition, TIRF imaging of spatiotemporal Ca^{2+} events that occur in the junctional structures of the plasmalemma specific to Ca^{2+} signal sites (or Ca^{2+} microdomain) has facilitated a deeper understanding on the cellular mechanisms underlying the local microdomain at the plasmalemmal and subplasmalemmal regions. Furthermore, accurate determinations of the distribution, dynamic behavior, subunit composition, stoichiometry, and interacting proteins of ion channels *in vitro* have been directly linked to understanding channel function and developing effective therapeutic drugs. TIRF imaging will shed new light on insights into cell physiology and pharmacology in the future.

Conflicts of interest

The authors indicated no potential conflicts of interest.

Acknowledgments

We thank Dr. Susumu Ohya (Kyoto Pharmaceutical University, Japan) for reading of this manuscript. This investigation was supported by a Grant-in-Aid for Scientific Research on Priority Areas from the Ministry of Education, Culture, Sports, Science, and Technology (25136717; to Y.I.) and Grant-in-Aids for Scientific Research (B) (26293021; to Y.I.), Scientific Research (C) (25460104; to H.Y.), and Young Scientists (B) (26860059; to Y. S.) from the Japan Society for the Promotion of Science. This work was also supported by a Grant-in-Aid from Takeda Science Foundation (to H.Y.).

References

(1) Axelrod D. Total internal reflection fluorescence microscopy in cell biology. Traffic. 2001;2:764–774.
(2) Giepmans BN, Adams SR, Ellisman MH, Tsien RY. The fluorescent toolbox for assessing protein location and function. Science. 2006;312:217–224.
(3) Ishijima A, Yanagida T. Single molecule nanobioscience. Trends Biochem Sci. 2001;26:438–444.
(4) Kusumi A, Tsunoyama TA, Hirosawa KM, Kasai RS, Fujiwara TK. Tracking single molecules at work in living cells. Nat Chem Biol. 2014;10:524–532.
(5) Ohara-Imaizumi M, Nishiwaki C, Kikuta T, Nagai S, Nakamichi Y, Nagamatsu S. TIRF imaging of docking and fusion of single insulin granule motion in primary rat pancreatic β-cells: different behaviour of granule motion between normal and Goto-Kakizaki diabetic rat β-cells. Biochem J. 2004;381:13–18.
(6) Pochynyuk O, Staruschenko A, Bugaj V, Lagrange L, Stockand JD. Quantifying RhoA facilitated trafficking of the epithelial Na^+ channel toward the plasma membrane with total internal reflection fluorescence-fluorescence recovery after photobleaching. J Biol Chem. 2007;282:14576–14585.
(7) Bezzerides VJ, Ramsey IS, Kotecha S, Greka A, Clapham DE. Rapid vesicular translocation and insertion of TRP channels. Nat Cell Biol. 2004;6:709–720.
(8) Lambers TT, Oancea E, de Groot T, Topala CN, Hoenderop JG, Bindels RJ. Extracellular pH dynamically controls cell surface delivery of functional TRPV5 channels. Mol Cell Biol. 2007;27:1486–1494.
(9) Veliz LA, Toro CA, Vivar JP, Arias LA, Villegas J, Castro MA, et al. Near-membrane dynamics and capture of TRPM8 channels within transient confinement domains. PLoS One. 2010;5:e13290.
(10) Haggie PM, Kim JK, Lukacs GL, Verkman AS. Tracking of quantum dot-labeled CFTR shows near immobilization by C-terminal PDZ interactions. Mol Biol Cell. 2006;17:4937–4945.
(11) Jin S, Haggie PM, Verkman AS. Single-particle tracking of membrane protein diffusion in a potential: simulation, detection, and application to confined diffusion of CFTR Cl^- channels. Biophys J. 2007;93:1079–1088.
(12) Notelaers K, Rocha S, Paesen R, Smisdom N, De Clercq B, Meier JC, et al. Analysis of α3 GlyR single particle tracking in the cell membrane. Biochim Biophys Acta. 2014;1843:544–553.
(13) Crane JM, Van Hoek AN, Skach WR, Verkman AS. Aquaporin-4 dynamics in orthogonal arrays in live cells visualized by quantum dot single particle tracking. Mol Biol Cell. 2008;19:3369–3378.
(14) Crane JM, Verkman AS. Long-range nonanomalous diffusion of quantum dot-labeled aquaporin-1 water channels in the cell plasma membrane. Biophys J. 2008;94:702–713.
(15) Nechyporuk-Zloy V, Dieterich P, Oberleithner H, Stock C, Schwab A. Dynamics of single potassium channel proteins in the plasma membrane of migrating cells. Am J Physiol Cell Physiol. 2008;294:C1096–C1102.
(16) Yamamura H, Ikeda C, Suzuki Y, Ohya S, Imaizumi Y. Molecular assembly and dynamics of fluorescent protein-tagged single $K_{Ca}1.1$ channel in expression system and vascular smooth muscle cells. Am J Physiol Cell Physiol. 2012;302:C1257–C1268.
(17) Ide T, Takeuchi Y, Aoki T, Yanagida T. Simultaneous optical and electrical recording of a single ion-channel. Jpn J Physiol. 2002;52:429–434.
(18) Ishikawa-Ankerhold HC, Ankerhold R, Drummen GP. Advanced fluorescence microscopy techniques–FRAP, FLIP, FLAP, FRET and FLIM. Molecules. 2012;17:4047–4132.
(19) O'Connell KM, Rolig AS, Whitesell JD, Tamkun MM. Kv2.1 potassium channels are retained within dynamic cell surface microdomains that are defined by a perimeter fence. J Neurosci. 2006;26:9609–9618.
(20) Di Biase V, Tuluc P, Campiglio M, Obermair GJ, Heine M, Flucher BE. Surface traffic of dendritic $Ca_V1.2$ calcium channels in hippocampal neurons. J Neurosci. 2011;31:13682–13694.
(21) Peran M, Hicks BW, Peterson NL, Hooper H, Salas R. Lateral mobility and anchoring of recombinant $GABA_A$ receptors depend on subunit composition. Cell Motil Cytoskelet. 2001;50:89–100.
(22) Notelaers K, Smisdom N, Rocha S, Janssen D, Meier JC, Rigo JM, et al. Ensemble and single particle fluorimetric techniques in concerted action to study the diffusion and aggregation of the glycine receptor α3 isoforms in the cell plasma membrane. Biochim Biophys Acta. 2012;1818:3131–3140.
(23) Won S, Kim HD, Kim JY, Lee BC, Chang S, Park CS. Movements of individual BK_{Ca} channels in live cell membrane monitored by site-specific labeling using quantum dots. Biophys J. 2010;99:2853–2862.
(24) Tamkun MM, O'Connell KM, Rolig AS. A cytoskeletal-based perimeter fence selectively corrals a sub-population of cell surface Kv2.1 channels. J Cell Sci. 2007;120:2413–2423.
(25) Bürli T, Baer K, Ewers H, Sidler C, Fuhrer C, Fritschy JM. Single particle tracking of α7 nicotinic AChR in hippocampal neurons reveals regulated confinement at glutamatergic and GABAergic perisynaptic sites. PLoS One. 2010;5:e11507.
(26) Meier J, Vannier C, Serge A, Triller A, Choquet D. Fast and reversible trapping of surface glycine receptors by gephyrin. Nat Neurosci. 2001;4:253–260.
(27) Lu R, Alioua A, Kumar Y, Eghbali M, Stefani E, Toro L. MaxiK channel partners: physiological impact. J Physiol. 2006;570:65–72.
(28) Tanaka Y, Koike K, Alioua A, Shigenobu K, Stefani E, Toro L. β1-subunit of MaxiK channel in smooth muscle: a key molecule which tunes muscle mechanical activity. J Pharmacol Sci. 2004;94:339–347.
(29) Wang L, Sigworth FJ. Structure of the BK potassium channel in a lipid membrane from electron cryomicroscopy. Nature. 2009;461:292–295.
(30) Korovkina VP, Brainard AM, Ismail P, Schmidt TJ, England SK. Estradiol binding to maxi-K channels induces their down-regulation via proteasomal degradation. J Biol Chem. 2004;279:1217–1223.
(31) Vogel SS, Thaler C, Koushik SV. Fanciful FRET. Sci STKE. 2006;2006. re2.
(32) Khakh BS, Fisher JA, Nashmi R, Bowser DN, Lester HA. An angstrom scale interaction between plasma membrane ATP-gated $P2X_2$ and $\alpha_4\beta_2$ nicotinic channels measured with fluorescence resonance energy transfer and total internal reflection fluorescence microscopy. J Neurosci. 2005;25:6911–6920.
(33) Bal M, Zhang J, Zaika O, Hernandez CC, Shapiro MS. Homomeric and heteromeric assembly of KCNQ (Kv7) K^+ channels assayed by total internal reflection fluorescence/fluorescence resonance energy transfer and patch clamp analysis. J Biol Chem. 2008;283:30668–30676.
(34) Schindl R, Frischauf I, Kahr H, Fritsch R, Krenn M, Derndl A, et al. The first ankyrin-like repeat is the minimum indispensable key structure for functional

assembly of homo- and heteromeric TRPC4/TRPC5 channels. Cell Calcium. 2008;43:260–269.
(35) Staruschenko A, Jeske NA, Akopian AN. Contribution of TRPV1-TRPA1 interaction to the single channel properties of the TRPA1 channel. J Biol Chem. 2010;285:15167–15177.
(36) Suzuki Y, Yamamura H, Ohya S, Imaizumi Y. Caveolin-1 facilitates the direct coupling between large conductance Ca^{2+}-activated K^+ (BK_{Ca}) and Cav1.2 Ca^{2+} channels and their clustering to regulate membrane excitability in vascular myocytes. J Biol Chem. 2013;288:36750–36761.
(37) Riven I, Kalmanzon E, Segev L, Reuveny E. Conformational rearrangements associated with the gating of the G protein-coupled potassium channel revealed by FRET microscopy. Neuron. 2003;38:225–235.
(38) Riven I, Iwanir S, Reuveny E. GIRK channel activation involves a local rearrangement of a preformed G protein channel complex. Neuron. 2006;51:561–573.
(39) Fowler CE, Aryal P, Suen KF, Slesinger PA. Evidence for association of $GABA_B$ receptors with Kir3 channels and regulators of G protein signalling (RGS4) proteins. J Physiol. 2007;580:51–65.
(40) Bal M, Zaika O, Martin P, Shapiro MS. Calmodulin binding to M-type K^+ channels assayed by TIRF/FRET in living cells. J Physiol. 2008;586:2307–2320.
(41) Bal M, Zhang J, Hernandez CC, Zaika O, Shapiro MS. Ca^{2+}/calmodulin disrupts AKAP79/150 interactions with KCNQ (M-Type) K^+ channels. J Neurosci. 2010;30:2311–2323.
(42) Kobrinsky E, Abrahimi P, Duong SQ, Thomas S, Harry JB, Patel C, et al. Effect of $Ca_V\beta$ subunits on structural organization of $Ca_V1.2$ calcium channels. PLoS One. 2009;4:e5587.
(43) Suzuki Y, Yamamura H, Ohya S, Imaizumi Y. Direct molecular interaction of caveolin-3 with KCa1.1 channel in living HEK293 cell expression system. Biochem Biophys Res Commun. 2013;430:1169–1174.
(44) Xie L, Kang Y, Liang T, Dolai S, Xie H, Parsaud L, et al. RalA GTPase tethers insulin granules to L- and R-type calcium channels through binding $\alpha 2\delta$-1 subunit. Traffic. 2013;14:428–439.
(45) Ulbrich MH, Isacoff EY. Subunit counting in membrane-bound proteins. Nat Methods. 2007;4:319–321.
(46) Kim EY, Rumpf CH, Van Petegem F, Arant RJ, Findeisen F, Cooley ES, et al. Multiple C-terminal tail Ca^{2+}/CaMs regulate $Ca_V1.2$ function but do not mediate channel dimerization. EMBO J. 2010;29:3924–3938.
(47) Nakajo K, Ulbrich MH, Kubo Y, Isacoff EY. Stoichiometry of the KCNQ1-KCNE1 ion channel complex. Proc Natl Acad Sci U. S. A. 2010;107:18862–18867.
(48) Penna A, Demuro A, Yeromin AV, Zhang SL, Safrina O, Parker I, et al. The CRAC channel consists of a tetramer formed by stim-induced dimerization of Orai dimers. Nature. 2008;456:116–120.
(49) Bartoi T, Augustinowski K, Polleichtner G, Gründer S, Ulbrich MH. Acid-sensing ion channel (ASIC) 1a/2a heteromers have a flexible 2:1/1:2 stoichiometry. Proc Natl Acad Sci U. S. A. 2014;111:8281–8286.
(50) Yu Y, Ulbrich MH, Li MH, Dobbins S, Zhang WK, Tong L, et al. Molecular mechanism of the assembly of an acid-sensing receptor ion channel complex. Nat Commun. 2012;3:1252.
(51) Bharill S, Fu Z, Palty R, Isacoff EY. Stoichiometry and specific assembly of best ion channels. Proc Natl Acad Sci U. S. A. 2014;111:6491–6496.
(52) Durisic N, Godin AG, Wever CM, Heyes CD, Lakadamyali M, Dent JA. Stoichiometry of the human glycine receptor revealed by direct subunit counting. J Neurosci. 2012;32:12915–12920.
(53) Tombola F, Ulbrich MH, Isacoff EY. The voltage-gated proton channel Hv1 has two pores, each controlled by one voltage sensor. Neuron. 2008;58:546–556.
(54) Demuro A, Penna A, Safrina O, Yeromin AV, Amcheslavsky A, Cahalan MD, et al. Subunit stoichiometry of human Orai1 and Orai3 channels in closed and open states. Proc Natl Acad Sci U. S. A. 2011;108:17832–17837.
(55) Ji W, Xu P, Li Z, Lu J, Liu L, Zhan Y, et al. Functional stoichiometry of the unitary calcium-release-activated calcium channel. Proc Natl Acad Sci U. S. A. 2008;105:13668–13673.
(56) Haggie PM, Verkman AS. Monomeric CFTR in plasma membranes in live cells revealed by single molecule fluorescence imaging. J Biol Chem. 2008;283:23510–23513.
(57) Bankston JR, Camp SS, Dimaio F, Lewis AS, Chetkovich DM, Zagotta WN. Structure and stoichiometry of an accessory subunit TRIP8b interaction with hyperpolarization-activated cyclic nucleotide-gated channels. Proc Natl Acad Sci U. S. A. 2012;109:7899–7904.
(58) Yu Y, Ulbrich MH, Li MH, Buraei Z, Chen XZ, Ong AC, et al. Structural and molecular basis of the assembly of the TRPP2/PKD1 complex. Proc Natl Acad Sci U. S. A. 2009;106:11558–11563.
(59) Pedemonte N, Galietta LJ. Structure and function of TMEM16 proteins (anoctamins). Physiol Rev. 2014;94:419–459.
(60) Kitamura K, Yamazaki J. Chloride channels and their functional roles in smooth muscle tone in the vasculature. Jpn J Pharmacol. 2001;85:351–357.
(61) Ohshiro J, Yamamura H, Saeki T, Suzuki Y, Imaizumi Y. The multiple expression of Ca^{2+}-activated Cl^- channels via homo- and hetero-dimer formation of TMEM16A splicing variants in murine portal vein. Biochem Biophys Res Commun. 2014;443:518–523.
(62) Cheng H, Lederer WJ. Calcium sparks. Physiol Rev. 2008;88:1491–1545.
(63) Demuro A, Parker I. "Optical patch-clamping": single-channel recording by imaging Ca^{2+} flux through individual muscle acetylcholine receptor channels. J Gen Physiol. 2005;126:179–192.
(64) Santana LF, Navedo MF, Amberg GC, Nieves-Cintron M, Votaw VS, Ufret-Vincenty CA. Calcium sparklets in arterial smooth muscle. Clin Exp Pharmacol Physiol. 2008;35:1121–1126.
(65) Luik RM, Wu MM, Buchanan J, Lewis RS. The elementary unit of store-operated Ca^{2+} entry: local activation of CRAC channels by STIM1 at ER-plasma membrane junctions. J Cell Biol. 2006;174:815–825.
(66) Imaizumi Y, Torii Y, Ohi Y, Nagano N, Atsuki K, Yamamura H, et al. Ca^{2+} images and K^+ current during depolarization in smooth muscle cells of the guinea-pig vas deferens and urinary bladder. J Physiol. 1998;510:705–719.
(67) Ohi Y, Yamamura H, Nagano N, Ohya S, Muraki K, Watanabe M, et al. Local Ca^{2+} transients and distribution of BK channels and ryanodine receptors in smooth muscle cells of guinea-pig vas deferens and urinary bladder. J Physiol. 2001;534:313–326.
(68) Morimura K, Ohi Y, Yamamura H, Ohya S, Muraki K, Imaizumi Y. Two-step Ca^{2+} intracellular release underlies excitation-contraction coupling in mouse urinary bladder myocytes. Am J Physiol Cell Physiol. 2006;290:C388–C403.
(69) Hotta S, Yamamura H, Ohya S, Imaizumi Y. Methyl-β-cyclodextrin prevents Ca^{2+}-induced Ca^{2+} release in smooth muscle cells of mouse urinary bladder. J Pharmacol Sci. 2007;103:121–126.
(70) Yamamura H, Imaizumi Y. Total internal reflection fluorescence imaging of Ca^{2+}-induced Ca^{2+} release in mouse urinary bladder smooth muscle cells. Biochem Biophys Res Commun. 2012;427:54–59.
(71) Imaizumi Y, Ohi Y, Yamamura H, Ohya S, Muraki K, Watanabe M. Ca^{2+} spark as a regulator of ion channel activity. Jpn J Pharmacol. 1999;80:1–8.
(72) Jaggar JH, Porter VA, Lederer WJ, Nelson MT. Calcium sparks in smooth muscle. Am J Physiol Cell Physiol. 2000;278:C235–C256.
(73) Ohno A, Ohya S, Yamamura H, Imaizumi Y. Regulation of ryanodine receptor-mediated Ca^{2+} release in vas deferens smooth muscle cells. J Pharmacol Sci. 2009;110:78–86.
(74) Yamazaki D, Tabara Y, Kita S, Hanada H, Komazaki S, Naitou D, et al. TRIC-A channels in vascular smooth muscle contribute to blood pressure maintenance. Cell Metab. 2011;14:231–241.
(75) Yamamura H, Cole WC, Kita S, Hotta S, Murata H, Suzuki Y, et al. Overactive bladder mediated by accelerated Ca^{2+} influx mode of Na^+/Ca^{2+} exchanger in smooth muscle. Am J Physiol Cell Physiol. 2013;305:C299–C308.